A New Proposal to Jefferson Lab PAC48

Measurement of the Two-Photon Exchange Contribution to the Electron-Neutron Elastic Scattering Cross Section

S. Alsalmi (spokesperson)

King Saud University, Riyadh 11451, Saudi Arabia

E. Fuchey (spokesperson) and A.J.R. Puckett

University of Connecticut, Storrs, Connecticut 06269, USA

B. Wojtsekhowski (spokesperson), S. Barcus, A. Camsonne, J-P. Chen,
D. Gaskell, J.-O. Hansen, D. W. Higinbotham, M. Jones, C. Keppel, D. Mack,
D. Meekins, R. Michaels, B. Sawatzky, G. Smith, A. Tadepalli, and S. Wood

Thomas Jefferson National Accelerator Facility, Newport News, Virginia 23606, USA

K. Aniol

California State University, Los Angeles, CA 90032, USA

D. Armstrong, T. Averett, M. Satnik, Z. Wertz, and B. Yale

The College of William and Mary, Williamsburg, Virginia 23185, USA

J. Arrington and P. Reimer

Argonne National Laboratory, 9700 S Cass Ave, Lemont, Illinois 60439, USA

C. Ayerbe Gayoso, H. Bhatt, D. Bhetuwal, B. Devkota,
J. Dunne, D. Dutta, L. El-Fassi, and A. Karki

Mississippi State University, Mississippi State, MS 39762, USA

V. Bellini

Istituto Nazionale di Fisica Nucleare, I-95123 Catania, Italy

J. Bernauer

Stony Brook University, Stony Brook, NY 11794, US

Riken BNL Research Center, Upton, NY 11973, US

D. Biswas, M. E. Christy, B. Dongwi, I. P. Fernando, T. Gautam,

M. Kohl, A. Nadeeshani, J. Nazeer, T. Patel, and M. Rathnayake

Hampton University, Hampton, Virginia 23669, USA

W. Boeglin and P. Markowitz

Florida International University, Miami, FL 33199, USA

G. Cates, K. Gnanvo, N. Liyanage, and V. Nelyubin

University of Virginia, Charlottesville, Virginia 232904, USA

E. Cline

Stony Brook University, Stony Brook, NY 11794, US

E. Cisbani, F. Meddi, and G. Urciuoli

Istituto Nazionale di Fisica Nucleare - Sezione di Roma,

P.le Aldo Moro, 2 - 00185 Roma, Italy

J.C. Cornejo* and B. Quinn

Carnegie Mellon University, Pittsburgh, Pennsylvania 15213, USA

D. Hamilton and R. Montgomery

SUPA School of Physics and Astronomy,

University of Glasgow, Glasgow G12 8QQ, UK

F. Hauenstein

Old Dominion University, Norfolk, Virginia 23529, USA

T. J. Hobbs

Department of Physics, Southern Methodist University, Dallas, TX 75275, USA

Jefferson Lab, EIC Center, Newport News, VA 23606, USA

A. T. Katramatou and G.G. Petratos

Kent State University, Kent, OH 44242, USA

T. Kutz and A. Schmidt

The George Washington University, Washington, DC 20052, USA

D. Nguyen

Massachusetts Institute of Technology, Cambridge, MA 02139, USA

C. Petta and C. Sutera

Istituto Nazionale di Fisica Nucleare, Sezione di Catania, I-95123 Catania, Italy

A. Sarty

Saint Mary's University, Halifax, Nova Scotia B3H 3C3, Canada

K. Slifer

University of New Hampshire, Durham, NH 03824, USA

A. Shahinyan

AANL, 2 Alikhanian Brothers Street, 0036, Yerevan, Armenia

W. Tireman

Northern Michigan University, Marquette, Michigan 49855, USA

(Dated: June 22, 2020)

(* - TBC)

Abstract

We propose to make a high precision measurement of the two-photon exchange contribution (TPE) in elastic electron-neutron scattering at a four-momentum transfer $Q^2 = 4.5$ $(\text{GeV/c})^2$. While significant efforts to study the two-photon-exchange have focused around elastic electron-proton scattering, the impact of TPE on neutron form factors was never examined experimentally. The proposed experiment will provide the very first assessment of the two-photon exchange in electron-neutron scattering, which will be important for understanding the nucleon form factor physics.

The proposed experiment will be performed in Hall A using the BigBite (BB) spectrometer to detect the scattered electrons and the Super-BigBite (SBS) to detect the protons and neutrons. The experiment should run concurrently with the E12-09-019 G_M^n and E12-17-004 G_E^n-Recoil experiments, which are expected to run in 2021. The experimental setup of the proposed experiment will be identical to that of E12-09-019 experiment.

The "ratio" method will be used to extract the electric form factor of the neutron G_E^n by scattering unpolarized electrons from deuterium quasi-elastically at two beam energies 4.4 and 6.6 GeV and electron scattering angles 41.9 and 23.3 degrees respectively. In the proposed approach, systematic errors are greatly reduced compared to those in the traditional single electron arm configuration. Several experiments at Mainz and JLab have used the ratio method to measure the neutron magnetic form factor in the past years. The method can be extended to extract the neutron electric form factor even with less stringent requirements on the knowledge of the absolute neutron detection efficiency and experimental kinematics than required for neutron magnetic form factor measurements.

I. INTRODUCTION

In 1950s, a series of experiments performed by R. Hofstadter [1] revealed that nucleons have a substructure (which corresponds to our modern view in terms of quarks and gluons). The experiment confirmed M. Rosenbluth's theory of electron scattering [2] based on the one-photon exchange approximation. In this so-called Born approximation, where the interaction between the electron and the nucleon occurs *via* an exchange of one virtual photon (OPE), the unpolarized $e - N$ elastic cross section can be parameterized in terms of a nucleon magnetic, G_M, and electric, G_E, form factors. These form factors describe the deviation from a point-like scattering cross section, σ_{Mott}:

$$\left(\frac{d\sigma}{d\Omega}\right)_{eN \to eN} = \frac{\sigma_{Mott}}{\epsilon(1+\tau)} \; \left[\tau \cdot G_M^2(Q^2) + \epsilon \cdot G_E^2(Q^2)\right], \tag{1}$$

where E and E' are the incident and scattered electron energies, respectively, θ is the electron scattering angle, $\tau \equiv -q^2/4M^2$, with $-q^2 \equiv Q^2 = 4EE' \sin(\theta/2)$ being the negative four momentum transfer squared, M is the nucleon mass, and $\epsilon = \left[1 + 2(1+\tau)\tan^2(\theta/2)\right]^{-1}$ is the longitudinal polarization of the virtual photon. The reduced cross section is defined by:

$$\sigma_r \equiv \left(\frac{d\sigma}{d\Omega}\right) \cdot \frac{\epsilon(1+\tau)}{\sigma_{Mott}} \; = \tau \cdot G_M^2(Q^2) + \epsilon \cdot G_E^2(Q^2) \; = \; \sigma_T + \epsilon \cdot \sigma_L, \tag{2}$$

where σ_L and σ_T are the cross sections for longitudinally and transversely polarized virtual photons, respectively.

The linear ϵ dependence of the cross section is due to the σ_L term. The ratio σ_L/σ_T is the so-called Rosenbluth slope related to G_E/G_M (in OPE), see Fig. 1. The data show that at Q^2 of 4-5 $(\text{GeV/c})^2$ the Rosenbluth slope is three to four times larger than expected in OPE (shown as the dot-dashed line in Fig. 1) for the observed values of the G_E^p/G_M^p ratio.

The nucleon electromagnetic form factors can reveal a lot of information about the nucleon internal structure, as well as the quark distribution. The form factors depend only on one variable, the negative square of the four-momentum transfer carried by the photon, Q^2. In
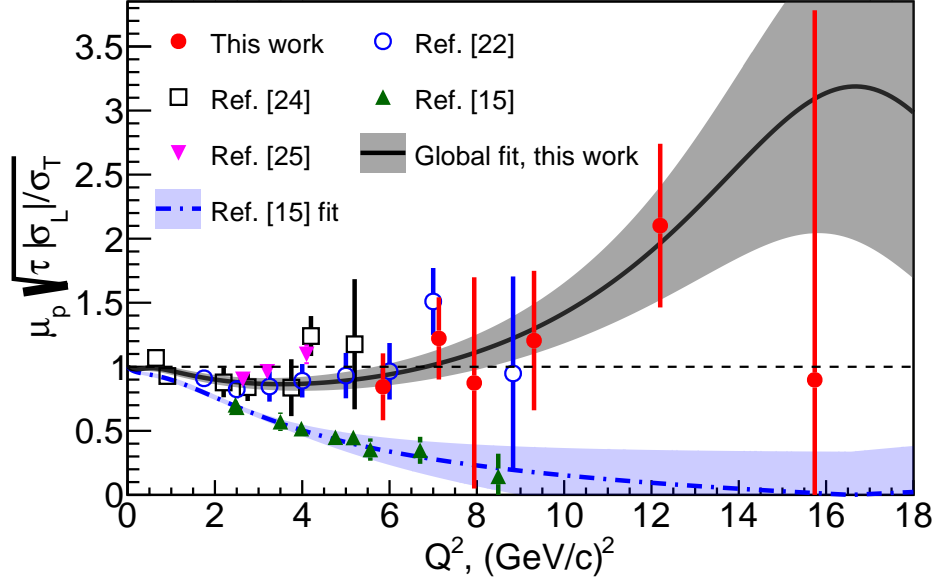
FIG. 1. The square root of Rosenbluth slope, corrected for kinematical factor $\sqrt{\tau}$ and μ_p, observed in elastic electron-proton scattering, adopted from Ref. [3]. References in the plot are also from Ref. [3]

24 the limit of large Q^2, perturbative QCD (pQCD) provides well-motivated predictions for the
25 Q^2-dependence of the form factors and their ratio. However, it was never predicted at what
26 Q^2 range the pQCD prediction (scaling) will be valid. Studies show that pQCD validity
27 will require a very large Q^2 of 100 $(\text{GeV/c})^2$. It was discovered at JLab, using the double
28 polarization methods, that the proton electric and magnetic form factors behave differently
29 starting at $Q^2 \approx 1$ $(\text{GeV/c})^2$.

30 Experimentally, the nucleon form factors can be measured using one of two techniques:
31 the polarization transfer technique and the Rosenbluth technique. The polarization method
32 examines the polarization transfer from longitudinally polarized electron to the recoiling
33 nucleon and determine the resulting azimuthal asymmetry distribution using a polarimeter.
34 Alternatively, one can use a polarized electron beam and polarized target. In the Rosenbluth
35 method, the electric and magnetic from factors can be separated by making two or more
36 measurements with different ϵ values (*i.e.* different beam energies and angles), but with same
37 Q^2 value. The Rosenbluth technique requires an accurate measurement of the cross section
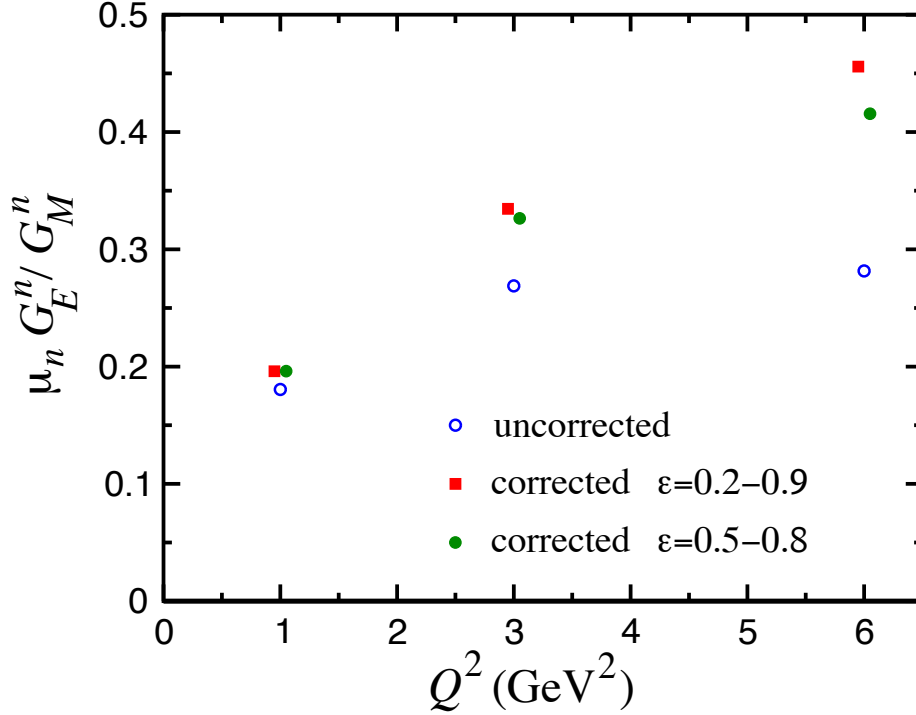
FIG. 2. Projected impact of TPE on G_E^n/G_M^n using LT separation, according to Ref. [4].

and suffers from large systematic uncertainties arising from several factors, for instance the need for a precise determination of the scattering angle. Additionally, for a measurement of the neutron form factors, accurate knowledge of the neutron detector efficiency is required, which is particularly hard to achieve. These uncertainties can be greatly reduced by measuring the ratio of $e-n$ and $e-p$ quasi-elastic cross sections.

When comparing the values of G_E^p/G_M^p obtained from both techniques, a significant discrepancy was observed (see Fig. 1). Such a discrepancy implies a potential problem in our understanding of the nucleon substructure. Many efforts were made to explain this effect, and it is believed that the inconsistency is due to the contribution of two-photon exchange in $e-N$ elastic scattering process [5, 6]. Predictions made for the neutron case are shown in Fig. 2 , adopted from [4]. The contribution of TPE could reach about 30% of the Rosenbluth slope value at 5 $(GeV/c)^2$.

⁵⁰   In the following we propose to make a precision L/T separation of the elastic electron-
⁵¹ neutron cross section and first experimental assessment of the two-photon exchange contri-
⁵² bution on the neutron magnetic form factor measurements (see also Ref. [7]). The result of
⁵³ the nTPE experiment will likely add a new component to our understanding of the elastic
⁵⁴ electron-nucleon process.

II. PHYSICS MOTIVATION

The nucleon plays the same central role in hadronic physics that the hydrogen atom does in atomic physics and the deuteron in the physics of nuclei. The structure of the nucleon and its specific properties, such as charge, magnetic moment, size, mass; the elastic electron scattering form factors, resonances; and structure functions in DIS, are of fundamental scientific interest. The isospin is a fundamental property of the nucleon, so both the proton and neutron investigations are important to do. By using data on the proton and neutron form factors the flavour structure could be explored [8]. It has already provided the most direct evidence for a diquark correlation in the nucleon [9–11].

Hadron structure, as seen in elastic electron scattering, in one-photon approximation, is defined by two functions of four momentum transfer square. They are: the helicity conserving Dirac form factor, F_1, which describes the distribution of the electric charge, and the helicity non-conserving Pauli form factor, F_2, which describes the distribution of the magnetic moment. These two form factors are the ingredients of the hadronic current. They contain information on the transverse charge distribution for an unpolarized and transversely polarized nucleon, respectively, in the infinite momentum frame [12, 13].

The Sachs form factors, G_E and G_M, the ratio of which will be extracted directly from the data, are related to F_1 and F_2 by

$$F_1 = \frac{G_E + \tau G_M}{1 + \tau} \text{ and } F_2 = \frac{G_M - G_E}{\kappa(1 + \tau)}, \tag{3}$$

where κ is the nucleon anomalous magnetic moment.

Already twenty-four years ago, an important development in QCD phenomenology has been the exploration of the generalized parton distribution (GPD) formalism [14–16], which provides relations between inclusive and exclusive observables. The nucleon elastic form factors F_1 and F_2 are given by the first moments of the GPDs

$$F_1(t) = \sum_q \int_0^1 H^q(x, \xi, t, \mu) dx \text{ and } F_2(t) = \sum_q \int_0^1 E^q(x, \xi, t, \mu) dx, \tag{4}$$

where H^q and E^q are two of the generalized parton distributions, x is the standard Bjorken x, ξ is is the "skewdness" of the reaction, t is the four-momentum transferred by the electron,

μ is a scale parameter necessary for the evolution over Q^2, analogous to DIS parton distributions, and the sum is over all quarks and anti-quarks. GPDs may be accessed through processes such as deeply virtual Compton scattering, where the interaction is factorized into a hard part with the virtual photon/photon interactions with an individual quark and a soft part of the residual system where the GPD information is contained.

A fundamental nucleon feature, the spin, is related to GPDs, as shown by X. Ji [15]. The moments of GPDs can yield information, according to Ji's Angular Momentum Sum Rule, on the contribution to the nucleon spin from quarks and gluons, including both the quark spin and orbital angular momentum.

At present, experimental measurements of GPDs are still scarce. Until high Q^2 DVCS data becomes available, work has been done to attempt to parameterize these GPDs, which rely heavily on data from electromagnetic form factors and parton distributions from DIS as constraints [17]. Data at high Q^2 for G_E^n would contribute significantly in the development of these models.

As we presented above, nucleon elastic form factors provide important input for the modeling of GPDs. At the same time, the measured cross section of elastic $e - p$ scattering at high Q^2 is significantly larger than predicted by Born-approximation calculations [18], indicating that TPE effects play a critical role in the high-Q^2 region and therefore must be well understood before conclusions about GPDs can be drawn.

III. TECHNIQUE

⁹⁹

This proposal is based on instrumentation, simulation, and analysis development made by the GMn/SBS collaboration for the GMn, E12-09-019, experiment [19]. The GMn experiment is one of several form factor experiments approved by JLab PAC. The SBS spectrometer was funded by DOE with large contributions provided by the collaborating institutions from USA, Italy, UK, and Canada. The apparatus and DAQ installation will start in 2020 and the data taking run is expected to be in summer-fall 2021.

The neutron form factors are challenging to be determine experimentally especially because there is no free neutron target. However, since deuterium is a loosely coupled system, it can be viewed as the sum of a proton target and a neutron target. In fact, quasi-elastic scattering from deuterium has been used to extract the neutron magnetic form factor, G_M^n, at modestly high Q^2 for decades [20, 21] in the single arm (e,e') experiments. However, the proton cross section needs to be subtracted by applying a single-arm quasi-elastic electron-proton scattering. This "proton-subtraction" technique suffers from a number of systematic uncertainties e.g. contributions from inelastic and secondary scattering processes.

Many years ago, L. Durand [22] proposed the so-called "ratio-method" based on the measurement of both D(e,e'n) and D(e,e'p) reactions. In this method, many of the systematic errors are canceled out. Several experiments [23–25] have applied the ratio-method to determine the neutron magnetic form factor.

The GMn/SBS experiment [19] will take data for elastic $e - n$ scattering for several kinematics with Q^2 from 3.5 up to 13.5 $(\text{GeV/c})^2$. We propose to use this method to measure the Rosenbluth slope and extract (in OPE approximation) the neutron electric form factor, G_E^n, at one value of momentum transfer. In fact, one of the required data points will be taken by the GMn experiment, so an additional measurement is needed only for one kinematics.

Data will be collected for quasi-elastic electron scattering from deuterium in the process $D(e, e'n)p$. Complementary $D(e, e'p)n$ data will be taken to calibrate the experiment apparatus. The current knowledge of the $e - p$ elastic scattering cross section (obtained in the single arm H(e,e')p and H(e,p)e' experiments) will be also used for precision determination the experiment kinematics.

Applying the Rosenbluth technique to measure G_E^n requires accurate measurement of the cross section and suffers from large uncertainties. To overcome this issue, we propose to extract the value of G_E^n from the ratio of quasi-elastic yields, $R_{n/p}$, in scattering from a deuteron target as follows:

$$R_{n/p} \equiv R_{observed} = \frac{N_{e,e'n}}{N_{e,e'p}} \qquad (5)$$

$R_{observed}$ needs to be corrected to extract the ratio of e-n/e-p scattering from nucleons:

$$R_{corrected} = f_{corr} \times R_{observed} \ , \qquad (6)$$

where the correction factor f_{corr} takes into account the variation in the hadron efficiencies due to changes of the $e - N$ Jacobian, the radiative corrections, and absorption in path from the target to the detector, and small re-scattering correction.

In one-photon approximation, $R_{corrected}$ can be presented as:

$$R_{corrected} = \frac{\sigma^n_{Mott} \cdot (1 + \tau_p)}{\sigma^p_{Mott} \cdot (1 + \tau_n)} \times \frac{\epsilon \sigma^n_L + \sigma^n_T}{\epsilon \sigma^p_L + \sigma^p_T} \qquad (7)$$

It is important that the ratio $R_{Mott} = \frac{\sigma^n_{Mott} \cdot (1+\tau_p)}{\sigma^p_{Mott} \cdot (1+\tau_n)}$ could be determine with very high relative accuracy even with modest precision for the beam energy, electron scattering angle, and detector solid angle. Now, let us write the $R_{corrected}$ at two values of ϵ using $S_c^{n(p)} = \sigma_L^{n(p)}/\sigma_T^{n(p)}$ as:

$$R_{corrected,\epsilon_1} = R_{Mott,\epsilon_1} \times \frac{\epsilon_1 \sigma^n_L + \sigma^n_T}{\epsilon_1 \sigma^p_L + \sigma^p_T} \qquad R_{corrected,\epsilon_2} = R_{Mott,\epsilon_2} \times \frac{\epsilon_2 \sigma^n_L + \sigma^n_T}{\epsilon_2 \sigma^p_L + \sigma^p_T}$$

In these two equations there are two unknown variables: σ^n_L and σ^n_T. We remind here that proton and neutron measurements are made simultaneously with the same apparatus. Thanks to this, the dominant contribution to the uncertainty of the Rosenbluth slope of the reduced cross section vs. ϵ, $S_c^n = \sigma^n_L/\sigma^n_T$, will come from the uncertainty of S_c^p. At Q^2=4.5 (GeV/c)^2, according to the global analysis of $e - p$ cross section [3], the value of S_c^p is close to $1/(\tau \mu_p^2) = 0.107$ with uncertainty of 0.01. The resulting equation for S_c^n is:

$$A = B \times \frac{1 + \epsilon_1 S_c^n}{1 + \epsilon_2 S_c^n} \approx B \times (1 + \Delta\epsilon \cdot S_c^n),$$

137 where the variable $A = R_{corrected,\epsilon_1}/R_{corrected,\epsilon_2}$ will be measured with statistical precision

138 of 0.1%. Assuming, for this estimate, equal values of Q^2 for two kinematics, the τ and σ_T for

139 two kinematics are canceled out, and the variable $B = R_{M,\epsilon_1}/R_{M,\epsilon_2} \times (1 + \epsilon_2 S_c^p)/(1 + \epsilon_1 S_c^p)$.

140 For actual small range of ϵ and small value of the slope, the $B \approx (1 - \Delta\epsilon \cdot S_c^p)$. The value

141 of B will be determined from global proton $e - p$ data to a precision of 0.25×0.01.

142 At Q^2=4.5 (GeV/c)^2 the ratio $\mu_n G_E^n/G_M^n$ is 0.55 ± 0.05 based on polarization transfer

143 data which is mostly insensitive to TPE, see review [26]. In the simplest model, the slope

144 S_c^n is a sum of the slope due to G_E^n/G_M^n and the TPE contribution. If we use for TPE the

145 prediction [4] which is reproduced on our Fig. 2, the TPE leads to increase of S_c^n by a factor

146 of 2, so the result of this experiment for TPE will be $0.069 \pm 0.012 \pm 0.01$, where the first

147 uncertainty is due to accuracy of G_E^n/G_M^n and the second one due to projected precision of

148 this experiment. It would be a 4-4.5 sigma observation of the neutron TPE.

IV.   PROPOSED MEASUREMENTS

We propose to use the same experimental setup of the E12-09-019 experiment. We will add a kinematic point at $Q^2 = 4.5$ $(\text{GeV/c})^2$, at a higher beam pass (6.6 GeV/3 pass instead of 4.4 GeV/2 pass), leading to a higher ϵ value. This additional point along with the data point of the E12-09-019 experiment will allow us to perform the standard Rosenbluth method to obtain (in one-photon approximation) the neutron electric and magnetic form factors. In addition, the ratio method (Sec.III), in which the systematic errors are greatly reduced, will be implemented to calculate the two photon exchange (TPE) contribution. The study of the ϵ dependence of the reduced cross section will help examine the two photon exchange contribution to the neutron form factor ratio G_E^n/G_M^n. Table. I displays the kinematic settings of the proposed experiment.

Point	Q^2 $(\text{GeV/c})^2$	E (GeV)	E' (GeV)	θ_{BB} degrees	θ_{SBS} degrees	ϵ
1	4.5	4.4	2.0	41.88	24.67	0.599
2	4.5	6.6	4.2	23.23	31.2	0.838

TABLE I. Kinematic settings of the proposed experiment. The kinematic point with the lowest ϵ value (blue row) is an existing measurement of the approved E12-09-019 experiment.

V.   EXPERIMENTAL SETUP

As illustrated in Fig. 3, this experiment will study electron scattering from a 15 cm long liquid Deuterium target held in a vacuum. The scattered electron will be detected in the BigBite spectrometer with an upgraded electron detector stack. The neutron arm is arranged with a dipole magnet 48D48 (SBS) and a segmented hadron calorimeter HCAL. The whole detector package was designed and is being assembled for the GMn, E12-09-019, experiment.
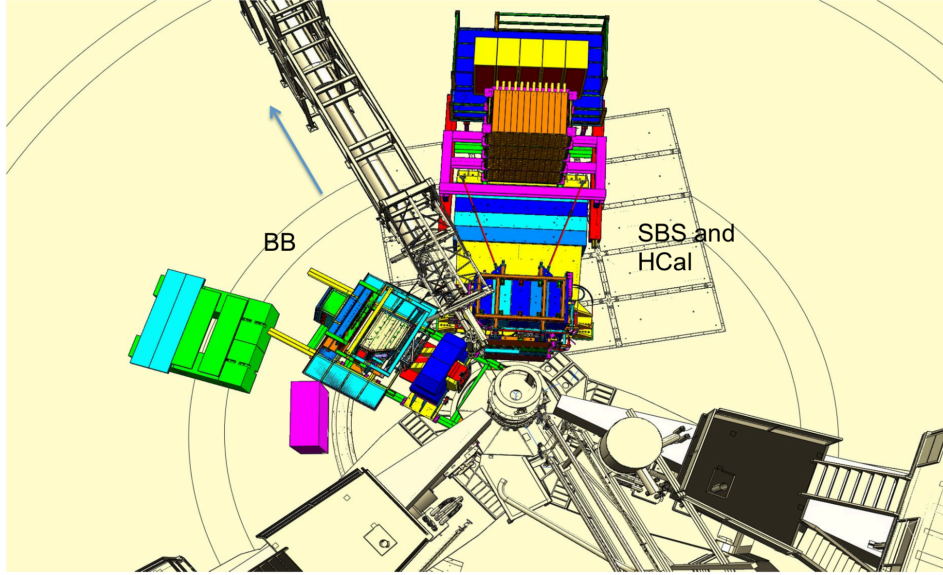

FIG. 3. Layout of the experimental setup in nTPE.

1.   Parameters of the SBS

The 48D48 magnet from Brookhaven was acquired as part of the Super Bigbite project and will be available for this experiment. It consists of a large dipole magnet which provides a field integral of about 1.7 $T \cdot m$, allowing for quasielastic protons to be sufficiently deflected to allow clear differentiation from neutrons. The active field volume has an opening of $46 \times$ 25 vertical $\times$ horizontal), matching the aspect ratio of the neutron arm, and a depth of 48 cm.

The placement of this magnet will be 1.6 m away from the target, which would normally

174 interfere with the beamline. To accommodate this, modifications were made to the iron yoke
175 such that the beamline will pass through the magnet yoke area.

176 The field configuration will be such that positively charged particles will be deflected
177 upwards away from the hall floor. For a field integral of 1.7 Tesla-m, protons of momentum
178 2.5 GeV/c will be deflected 250 mrad, which translates to a displacement of 1.29 m. Including
179 expected detector resolution, the $p_{miss,\perp}$ distribution will be similar to what was seen in
180 E02-013, so cuts of < 100 MeV/c will be appropriate. Monte Carlo simulations show a
181 contamination of charged quasielastics to be negligible.

182 The presence of the magnet also works to sweep low energy charged particles from the
183 target away from the neutron arm. Particles of momentum less than 1.3 GeV/c will be
184 entirely swept outside of the neutron arm acceptance. This greatly reduces the amount of
185 charged low energy background.

A. The BigBite Spectrometer

Scattered electrons will be detected in the BigBite spectrometer. The spectrometer consists of a single dipole magnet (with magnetic field approximately 1.2 T) and a detection system, see Fig. 4.
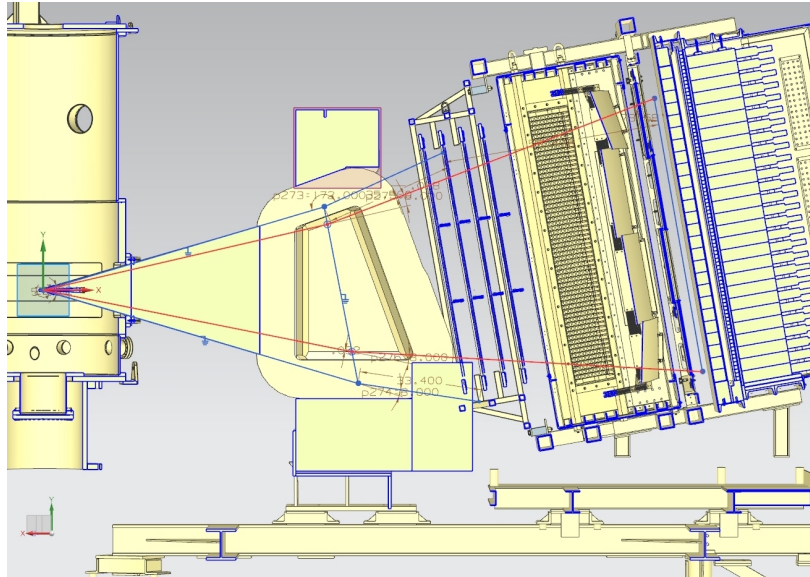

FIG. 4. The BigBite spectrometer with the upgraded detector stack.

1. GEM Chambers

To perform the tracking of charged particles under the high rates anticipated for this experiment, the drift chambers were replaced with gas electron multiplier (GEM) detectors. These detectors have proven to be capable of operating under luminosities of 25 kHz/mm^2 for the COMPASS experiment at CERN and the spatial resolution of each of these chambers is anticipated to be about 70 μm. There will be two sets of GEMs placed on each side of the GRINCH Cherenkov detector.

The set of GEMs in front of the GRINCH is composed of four layers of GEMs. Two of these layers have been built by the SBS collaborators from INFN. They are composed three

modules each, measuring 40×50 cm^2, such that each layer covers 40×150 cm^2 (the long dimension being vertical, along the dispersive direction). The readout of these modules are oriented in the x/y direction *i.e.* parallel and perpendicular to the dispersive direction (horizontal and vertical). The two other layers are being built by the SBS collaborators from UVA. They are composed of a single module measuring 40×150 cm^2, the long dimension again being vertical and along the dispersive direction. The readout of these modules are oriented in the u/v direction *i.e.* ± 30 degrees with respect to the horizontal direction.

The set of GEMs behind the GRINCH has been been built by the SBS collaborators from UVA. It is composed of a single layer composed of four modules measuring 50×60 cm^2, such that the layer covers 60×200 cm^2 (the long dimension again being along the dispersive direction). The readout of these modules are all oriented in the x/y direction.

The background levels in the GEMs have been evaluated, with the help of the G4SBS simulation package([27] and Sec. VI) for the G_M^n experimental readiness review. For the G_M^n highest Q^2 point (which is the most constraining, since it combines mandatory maximum luminosity and smaller BigBite angles), the rates in the front GEMs are of the order of 120 kHz/cm^2 for the front GEM layers, and below 50 kHz/cm^2 for the back GEM. To perform the GEM tracking within such a high-rate environment, we use the cluster reconstructed in the BigBite shower as a track seed to clean the large combinatorics that would otherwise be created by the large number of hits. After this, the main challenge is the separation by the clustering algorithm of the signal and background hits to minimize track smearing. At this level of background, a TreeSearch tracking algorithm combined with a fairly simple cluster separation algorithm has already proven to achieve 70% efficiency at nominal luminosity. A better cluster separation algorithm is currently being developed and should allow to significantly improve this figure.

2. *Shower/Preshower*

The electromagnetic calorimeter configuration consists of two planes of lead glass blocks which we call the preshower and shower. The preshower, located about 80 cm behind the first GEM chamber, consists of a 2×26 plane of 37 cm $\times$ 9 cm blocks. The shower, about

227 1 m behind the first GEM chamber, consists of an 7×27 array of 8.5 cm $\times$ 8.5 cm blocks.
228 Sums over these blocks form the physics event trigger for the experiment.

229 The preshower signal can be used to provide an additional method of pion rejection.
230 By selecting low preshower signals, a pion rejection factor of 1:50 can be achieved through
231 optimization. Despite higher particle rates, pion rejection performance is anticipated to
232 be similar to that achieved for Transversity, E06-010. By measuring the pedestal widths
233 and resolution for E06-010 and scaling to this proposal's conditions, overall relative energy
234 resolution for the detector is expected to become worse by a factor of 1.6, to about $\sigma_{\delta E/E} =$
235 25%.

3. Timing hodoscope

237 The BigBite timing hodoscope has been built by the SBS collaborators from Glasgow to
238 replace the BigBite scintillator plane. It will be composed of 90 bars stacked in a plane,
239 each with dimensions 1 in. $\times$ 1 in. $\times$ 60 cm. The paddle stack will be oriented such that
240 the long dimension of the bars is horizontal *i.e.* perpendicular to the dispersive direction.
241 Each of these elements are read out by a PMT on each side, mostly to provide measurement
242 redundancy.

243 This plane will primarily be used to provide a signal for nucleon time of flight reconstruc-
244 tion. A time resolution of 200 ps is anticipated. This fine segmentation is meant to lower the
245 rates in the detector. Background studies made for the G_M^n experimental readiness review
246 demonstrated that the rates experienced by each element was $\leq$ 500 kHz at a luminosity of
247 2.8 $\times 10^{38}$ cm^{-2} s^{-2}. Signals from the PMTs are processed by NINO front-end cards which,
248 when the PMT pulse crosses the NINO threshold, will produce a digital signal to be read
249 out by CAEN 1190 TDCs which record a leading time and a trailing time.

4. GRINCH cherenkov detector

251 The main purpose of the GRINCH is to provide additional particle identification for offline
252 pion rejection. The GRINCH consists of a tank with a maximum depth of 88.9 cm, with 4

cylindrical mirrors focusing the cherenkov light directly onto a 510 PMT array (60 lines of PMTs, with lines of 9 PMTs alternating with lines of 8 PMTs) placed away from the beam. The radiation gas will be C_4F_8, which is by far the best compromise between light yield for electrons and operating cost. With $n - 1 = 1.35 \times 10^{-3}$, the π threshold is only about 2.7 GeV, so the additional pion rejection will be most effective below this threshold.

Similar to the timing hodoscope, the signals from the GRINCH PMTs pulses are processed by NINO front-end cards which, when the PMT pulse crosses the NINO threshold, will produce a digital signal to be readout by VETROC TDCs, which for each PMT hit will record a leading time and a trailing time. The analog signal will not be recorded however, which means that for each PMT hit, the information of the number of photoelectrons is not directly available (although it can in theory be deduced from the time over threshold).

All of this implies that the electron selection relies on the number of GRINCH PMT firing, instead of relying on the signal amplitude.

B.   Hadron Calorimeter (HCal)

²⁶⁶

²⁶⁷ The Hadron Calorimeter (HCal) has been designed specifically to measure the recoil
²⁶⁸ nucleon for the SBS experiments. Specifically for this experiment (and for G_M^n), HCal
²⁶⁹ combined with the SBS (48D48) magnet provides identification of the recoil nucleon, as
²⁷⁰ well as additional kinematic constraint and possibly timing information on the measured
²⁷¹ interaction. Nucleon identification is illustrated on Fig. 5. This figure shows the compared
²⁷² proton and neutron position distribution in HCal at the same electron kinematics. The
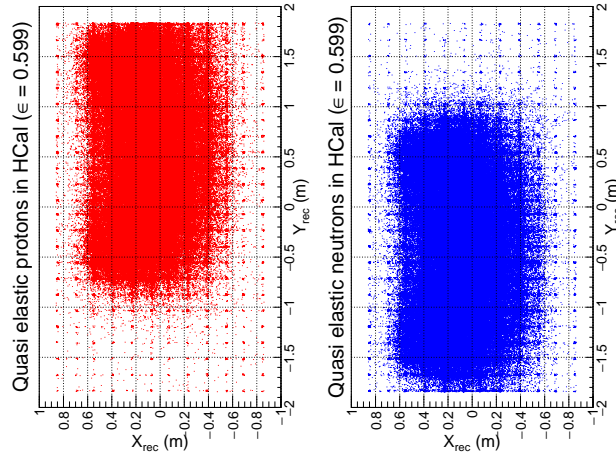²⁷³ proton distribution is being shifted upwards by about 1 m compared to the neutron.

FIG. 5. Reconstructed HCal cluster from quasi-elastic events generated by G4SBS. The left distri-
bution in red is for the proton, the right distribution in blue is for the neutron.

²⁷⁴ The HCal (a CAD model of which is shown in Fig. 6)is composed of 288 modules arranged
²⁷⁶ in an array of 12×24. In front of the full assembly is located a $3/4 -$ inch steel plate which
²⁷⁷ serves two purposes:

²⁷⁸ • initiate the hadronic shower to optimize the calorimeter response;

²⁷⁹ • shield the modules from a fraction of the low energy secondaries;

²⁸⁰ Each of these modules measures $6 \times 6 \, \text{in}^2$ section, for 3 ft length. They are composed of
²⁸¹ alternating tiles of scintillators and iron around a central light guide which collects the light
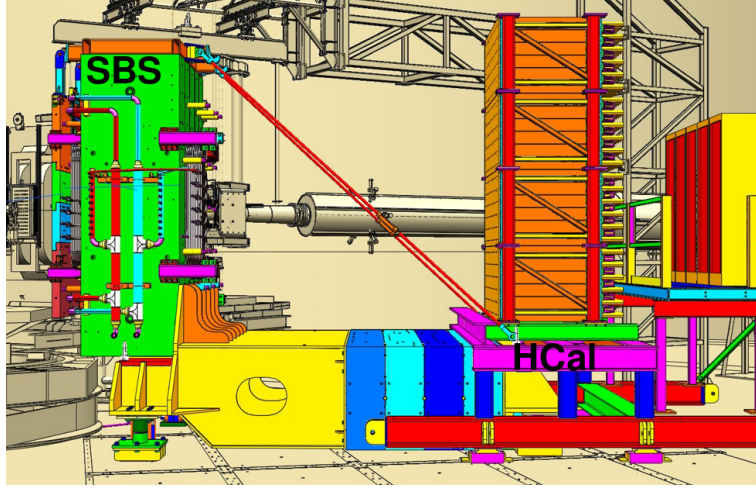
FIG. 6. CAD representation of HCal (right) with the SBS magnet (left)

generated in the scintillators by the hadronic shower, and guides it to the PMT at the end of the block. Cosmic tests have determined that the average light yield for the HCal modules is around 5 photoelectrons per MeV deposited in the scintillator tiles.

The PMTs are read out with FADC250 which sample the PMT signal every 4 ns and allow to reconstruct the PMT pulse shape, and hence its timing. They are also read out by TDCs which provide additional timing information. Thanks to this, the timing resolution can be better than 1 ns, which cosmics tests (in progress) seem to confirm.

The energy resolution is intrinsically broad (see Fig. 9 in Section VI), due mostly to the small fraction of energy from the hadronic shower actually measured by the scintillator tiles (≤ 0.1 - refer yet again to Fig. 9).

VI. SIMULATIONS, ESTIMATIONS OF COUNTING RATES AND ACCIDENTALS

The estimates of counting rates accidentals have been performed using G4SBS, the GEANT4-based simulation package developed for the SBS experiment [27]. This package includes a wide range of event generators, which allows us to evaluate the rates for both events of interest (signal) and background. The representation of the experiment apparatus in G4SBS is shown in the high ϵ configuration in Fig. 7.
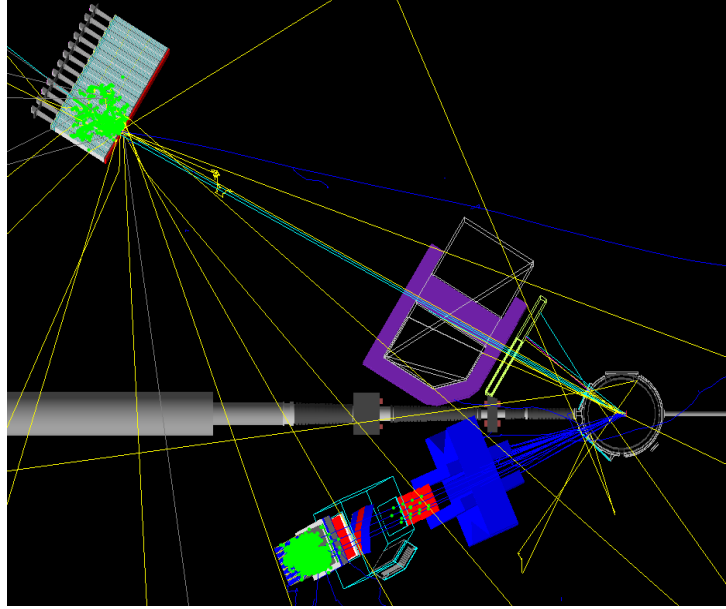

FIG. 7. Top view of the experimental apparatus model in G4SBS, shown in the high ϵ configuration. The beam direction is indicated, as well as the main elements (HCal, SBS magnet, BigBite spectrometer)

A. Background and trigger rates

The main processes expected to contribute to the trigger rates for the BigBite spectrometer are:

- the inelastic electron nucleon scattering process;

303 • photons from inclusive π^0 production;

304 • and to a lesser extent, charged pions.

305 Concerning HCal, various hadronic backgrounds are expected to contribute to the rates
306 in HCal, the dominant ones being pions. Both the inelastic scattering and the inclusive
307 neutral and charged pion production are implemented in G4SBS, the latter relying on the
308 Wiser parametrization [28]. The minimum-bias "beam-on-target" generator (including all
309 electromagnetic and hadronic processes) has also been considered for the HCal background.
310 The thresholds to apply to each arm are determined as a function of the elastic peak. For
311 the electron arm, the threshold has been set at $\mu_E - 2.5\sigma_E$, μ_E and σ_E being respectively
312 the position and width of the fitted elastic peak. Fig. 8 presents the distributions of rate of
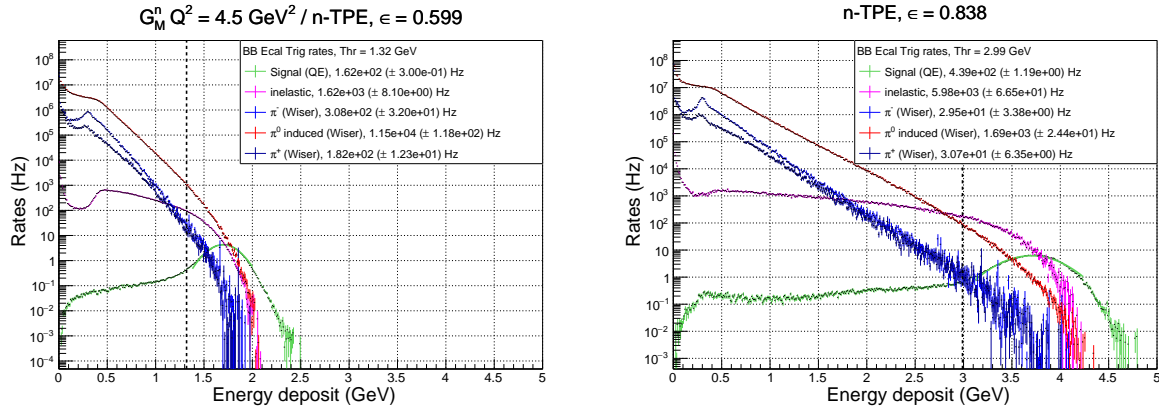313 energy deposit for the different processes involved in the BigBite trigger rates.

FIG. 8. Rates of the different process contributing to the BigBite electron arm trigger, for the low
ϵ (left) and the high ϵ (right). Quasi-elastic is in green, inelastic in magenta, $\pi 0$ in red, π^- in blue,
and π^+ in dark blue. Note the resolution for the elastic peak in the BigBite shower is ~ 0.3 GeV.

314 Since HCal is a sampling calorimeter (meaning that only a fraction of the shower energy
315 is measured), its resolution is relatively wide (~ 0.7 GeV). Due to this, the threshold is at
316 90% efficiency (which corresponds to $\sim$0.1 GeV for both kinematics. Fig. 9 presents the
317 distributions of rate of energy deposit for the different processes involved in the HCal trigger
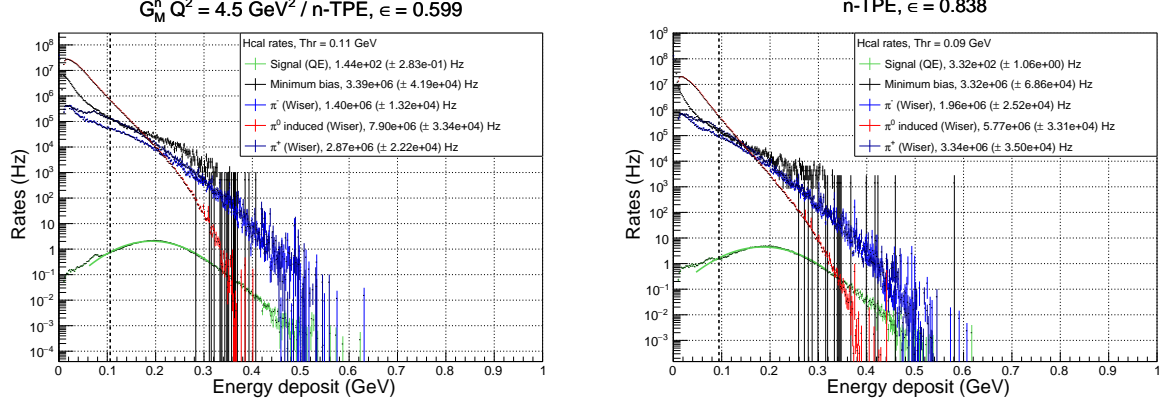318 rates.

FIG. 9. Rates of the different process contributing to the HCal trigger, for the low ϵ (left) and the high ϵ (right). Quasi-elastic is in green, minimum bias in black, $\pi 0$ in red, π^- in blue, and π^+ in dark blue. Note the peak itself is around 0.2 GeV for 3.2 GeV nucleons.

The thresholds and trigger rates for each arm, as well as the coincidence rate (assuming 30ns coincidence window), are summarized in Table. II. Note that for HCal, the "total rates" is either the "minimum bias" beam on target, *or* the sum of inclusive charged and neutral pions evaluated with the Wiser cross sections. Comparisons between Wiser and minimum bias at very low energy shows that the Wiser code results dramatically overestimate the HCal rates, henceforth the HCal rates estimations using minimum bias are deemed more reliable (and emphasized in Table. II). For the sake of thoroughness, we have checked the coincidence rates assuming the sum of the inclusive pions (evaluated with the Wiser cross sections) as the HCal rates.

Assuming this worst case scenario, the coincidence rates could be as high as 5kHz, which might be at the limit of manageability for the DAQ. However, even if those rates were proven to be accurate, a slight increase on the HCal threshold (which would drop the efficiency from $\sim$90% to $\sim$85%) would decrease the total HCal rates by $\sim$35% to 40% in this worst case scenario, which would make the situation more manageable (3.3 kHz). In the more reasonable case where the HCal rates are more accurately described by the minimum bias prediction, the coincidence will be lower than 2kHz, rate at which the SBS DAQ should operate safely.

Point (ϵ)	1 (0.599)		2 (0.838)	
	BigBite rates (Hz)	HCal rates (Hz)	BigBite rates (Hz)	HCal rates (Hz)
threshold (GeV)	1.32	0.106	2.99	0.090
Quasi-elastic	1.62×10^2	1.44×10^2	4.39×10^2	3.48×10^2
Inelastic	1.62×10^3	-	5.98×10^3	-
π^- (Wiser)	3.08×10^2	1.40×10^6	2.95×10^2	1.96×10^6
π^0 (Wiser)	1.15×10^4	7.90×10^6	1.69×10^3	5.77×10^6
π^+ (Wiser)	1.82×10^2	2.87×10^6	3.07×10^2	3.34×10^6
Minimum bias	-	3.39×10^6	-	$3.32 \times 10^6 (*)$
Total	1.37×10^4	3.39×10^6	8.17×10^3	3.32×10^6
($\sum_{\pi(Wiser)}$ for HCal)		/ (1.22×10^7)		/ (1.11×10^7)
Coincidence rate	1.39×10^3		8.14×10^2	
($\sum_{\pi(Wiser)}$ for HCal)	(5.01×10^3)		(2.72×10^3)	

TABLE II. Trigger rates for BigBite and HCal, with the different process contributions separated, and the sum. For HCal, the total rates is either estimated with the minimum bias generator or the sum of inclusive pions estimated with the Wiser cross section. The coincidence rates assume a 30 ns coincidence window.

B. Contamination from inelastic

The main source of contamination for the quasi-elastic comes from the inelastic electron-nucleon scattering. Most of this contamination can be cleaned out thanks to a selection on the center of mass energy

$$W^2 = M_N^2 + 2M_N^2(E - E') - Q^2, \tag{8}$$

and the missing transverse momentum of the nucleon

$$p_{\perp miss} = \sqrt{(q_x - p'_x)^2 + (q_y - p'_y)^2}, \tag{9}$$

where M_N is the mass of the nucleon, E and E' the initial and final energy of the electron, and $q_{x,y}$, $p'_{x,y}$ are the projections on x, y of the vectors of the virtual photon and final nucleon. The distributions of these quantities (weighted with cross section and including detector resolutions) are displayed for quasi-elastic and inelastic scattering, and for proton and nucleon, on Fig. 10 for the low ϵ kinematic, and on Fig. 11 for the high ϵ kinematic.

FIG. 10. Compared quasi-elastic and inelastic distributions (including detectors resolutions) for $p_{\perp miss}$ (top) and W^2 (bottom), for the low ϵ kinematic. Comparison for protons is on the left, and comparison for neutrons is on the right. On the bottom panel, black and red are before the $p_{\perp miss} \leq 0.1$ GeV selection, while blue and magenta are after $p_{\perp miss} \leq 0.1$ GeV selection and application of BigBite shower and HCal thresholds.

Provided that we are not limited by statistics and we prioritize sample purity is capital for our experiment, we set the selection criteria on W^2 and $p_{\perp miss}$ to minimize inelastic
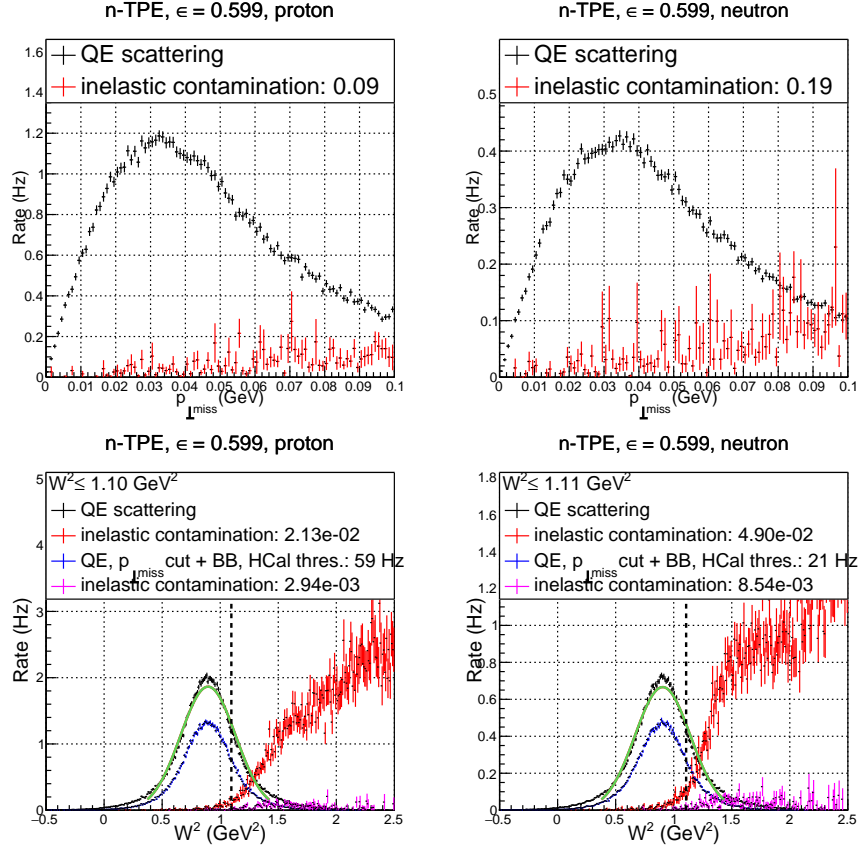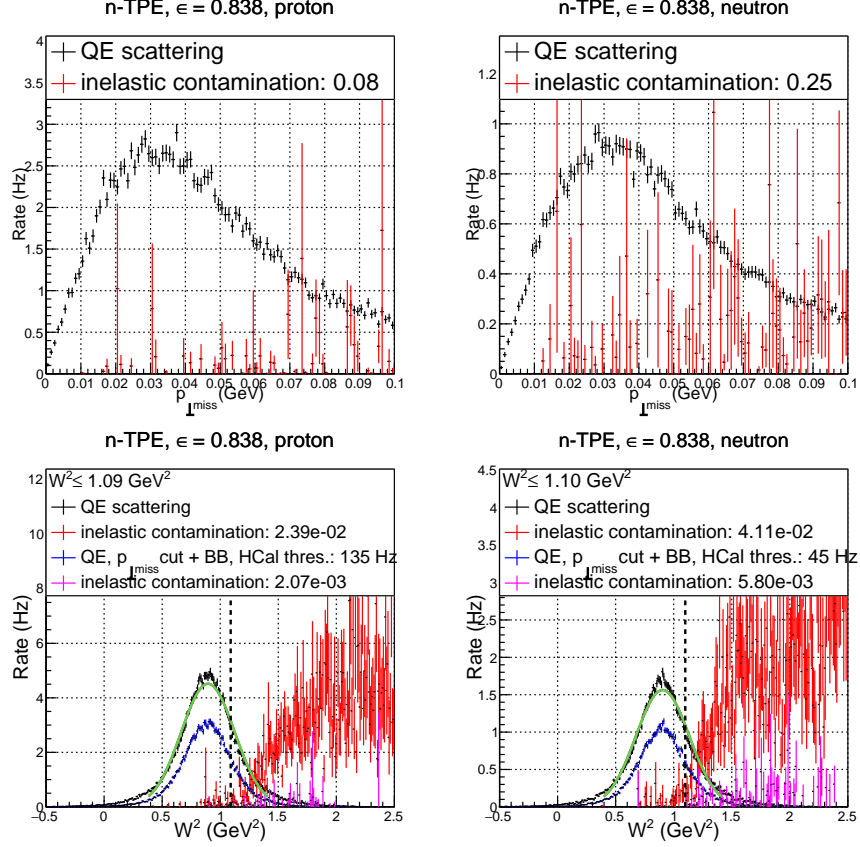
FIG. 11. Compared quasi-elastic and inelastic distributions (including detectors resolutions) for $p_{\perp miss}$ (top) and W^2 (bottom), for the high ϵ kinematic. Comparison for protons is on the left, and comparison for neutrons is on the right. On the bottom panel, black and red are before the $p_{\perp miss} \leq 0.1$ GeV selection, while blue and magenta are after $p_{\perp miss} \leq 0.1$ GeV selection and application of BigBite shower and HCal thresholds.

contamination (ideally below 1 %). Setting $p_{\perp miss} \leq 0.1$ GeV and $W^2 \leq 1.1$ GeV^2, the inelastic contamination of the elastic sample ranges from 0.2 % to 0.9 %, while retaining ≥ 60 % of the quasi-elastic events properly recorded in the BigBite-SBS pair. Table. III summarizes the quasi-elastic selection cuts, and inelastic contamination δ_{inel}.

Point (ϵ)	N	W^2 cut	$p_{\perp miss}$ cut	δ_{inel}
1 (0.599)	n	1.10	0.10	2.94×10^{-3}
	p	1.11	0.10	8.54×10^{-3}
2 (0.838)	n	1.09	0.10	2.07×10^{-3}
	p	1.10	0.10	5.80×10^{-3}

TABLE III. Summary of cuts for quasi-elastic selection and resulting inelastic contamination δ_{inel}.

C. Quasi-elastic counting rates

The signals for this experiment have been generated using the G4SBS elastic/quasi-elastic generator. We generated a reasonably large sample of quasi-elastic events N_{Gen} for each kinematics, within a solid angle $\Delta\Omega_{Gen}$ that was larger than the detector acceptance. To evaluate the detector solid angle, we define simple criteria that each event has to pass, defined as follows:

- require a primary track, going through all 5 GEM layers (electron arm);

- require non-zero energy deposit in both the preshower and shower (electron arm);

- require non-zero energy deposit in HCal (hadron arm).

The detector solid angle, for both proton and neutron, are defined in Table. IV. We also define there the *p-n* acceptance asymmetry $A_{\Delta\Omega}$ such as:

$$A_{\Delta\Omega} = \frac{(\Delta\Omega_e \otimes \Delta\Omega_n) - (\Delta\Omega_e \otimes \Delta\Omega_p)}{(\Delta\Omega_e \otimes \Delta\Omega_n) + (\Delta\Omega_e \otimes \Delta\Omega_p)} \tag{10}$$

Then, we evaluate the detection efficiency. For the electron, we require the energy reconstructed in the BigBite calorimeter to be above a threshold defined as $thr = \mu_E - 2.5 * \sigma_E$, as well as a minimum number of GRINCH PMTs fired due to the primary electron; For HCal, we select a threshold that yields 90% efficiency. These values are summarized in Table. V. Quasi-elastic selection efficiency η_{sel} are also provided.

The counting rates are evaluated using among the N_{Gen} events generated the events that have passed the selection described below, and weighting those events with the cross section

Point (ϵ)	$\Delta\Omega_e$ (msr)	$\Delta\Omega_e \otimes \Delta\Omega_n$ (msr)	$\Delta\Omega_e \otimes \Delta\Omega_p$ (msr)	$A_{\Delta\Omega}$ (%)
1 (0.599)	52.4	46.7	47.2	0.5
2 (0.838)	32.7	20.8	22.2	3.0

TABLE IV. Kinematics electron solid angle, and convoluted electron/hadron solid angle, and acceptance asymmetry.

Point (ϵ)	BB thr. (GeV)	HCal thr. (GeV)	$\eta_{det\ e}$	$\eta_{det\ n}$	$\eta_{det\ p}$	$\eta_{sel\ n}$	$\eta_{sel\ p}$
1 (0.599)	1.32	0.11	0.902	0.904	0.892	0.589	0.605
2 (0.838)	2.99	0.09	0.808	0.889	0.882	0.617	0.647

TABLE V. Kinematics electron thresholds, particle detection efficiencies (η_{det}), and efficiency of quasi-elastic selection η_{sel} separated for the proton and the neutron.

$d\sigma/d\Omega|_i$ calculated by G4SBS, multiplied by the generation solid angle $\Delta\Omega_{Gen}$, using the formula:

$$N_{est} = \frac{\mathcal{L}_{exp}\Delta t}{N_{Gen}} \times \sum_{i \in accepted\ evts} \left(\frac{d\sigma}{d\Omega}\bigg|_i \times \Delta\Omega_{Gen} \right) , \tag{11}$$

where Δt the running time and $\mathcal{L}_{exp}$ the experimental luminosity. $\mathcal{L}_{exp}$ can be calculated as follows:

$$\mathcal{L}_{exp} = \frac{I_{exp}}{q_e} \cdot L_{tgt} \cdot d_{tgt} \, \frac{\mathcal{N}_A}{m_D} , \tag{12}$$

where I_{exp} is the beam current, q_e is the electron charge, L_{tgt} and d_{tgt} are the target length and density respectively, N_A is Avogadro's number, and m_D is the deuterium mass number. Events are "accepted" if they meet the following criteria:

- the electron is in the BigBite acceptance;

- the electron passes the BigBite threshold defined in Table V and gives signal in the GRINCH;

- the nucleon is in the HCal acceptance and passes the HCal threshold defined in Table V;

382 • the event passes the quasi-elastic selection defined in the previous section *i.e.* $W^2 \leq 1.1 \text{ GeV}^2$

383 and $p_{\perp miss} \leq 0.10$ GeV.

384 The total quasi-elastic statistics N_{QE}, as well as the total form factor, F^2:

$$F^2 = \frac{N_{QE}}{\mathcal{L}_{exp} \cdot \Delta t \cdot d\sigma_{Mott}/d\Omega \cdot \Delta\Omega \cdot \eta} \qquad (13)$$

385 and its statistical error $\Delta F^2 = F^2/\sqrt{N_{QE}}$ are compiled for both kinematics in Table. VI,

386 assuming a running time $\Delta t = 12$ hours of running at a beam intensity of $I_{exp} = 30 \ \mu A$ on

387 a liquid deuterium target with length $l_{tgt} = 15$ cm and density $d_{tgt} = 0.169$ g.cm^{-3}. In

388 Eq. 13, $\Delta\Omega$ is the convoluted BigBite-HCal solid angle, and η is the product of all efficiencies

389 (detection efficiencies $\eta_{det} \times$ selection efficiency η_{sel}).

Point (ϵ)	N_{QE} (e-n)	N_{QE} (e-p)	F_n^2 ($\times 10^{-3}$)	ΔF_n^2 ($\times 10^{-6}$)	F_p^2 ($\times 10^{-3}$)	ΔF_p^2 ($\times 10^{-6}$)
1 (0.599)	9.07×10^5	2.55×10^6	0.99	1.04	2.73	1.70
2 (0.838)	1.94×10^6	5.83×10^6	0.72	0.52	1.93	0.80

TABLE VI. Quasi-elastic counting rates, and total form factor (defined in Eq. 11).

390 The calculation of the F_2 term requires the evaluation of the Mott cross section:

$$\sigma_{Mott} \equiv \frac{d\sigma_{Mott}}{d\Omega} = (\hbar c \alpha_{EM})^2 \frac{1}{4E^2} \left(\frac{\cos \theta_e/2}{\sin^2 \theta_e/2} \right)^2 \frac{E'}{E} \qquad (14)$$

391 The Mott cross section has been calculated with the weighted average of the electron variables

392 (momentum and polar angle).

Point (ϵ)	$\langle \theta_e \rangle$ (deg)	$\langle k' \rangle$ (GeV)	$\langle Q^2 \rangle$ (GeV^2)	σ_{Mott} (nb sr^{-1})
1 (0.599)	41.88	2.0	4.5	6.62
2 (0.838)	23.23	4.2	4.5	44.2

TABLE VII. The Mott cross section weighted average of kinematic variables over the BigBite acceptance.

VII. SYSTEMATIC ERRORS

In this section we will estimate (or set upper limits on) the contributions to the systematic uncertainty for this experiment. The sources of systematic uncertainties from the experimental setup (target, acceptance, inelastic contamination) were already estimated for the SBS G_M^n experiment proposal [19]. Note that a majority of the potential sources of systematic uncertainties (nuclear corrections, accidentals, radiative corrections, target density, etc) cancel in the ratio $R = f_{corr} \times N_{e,e'n}/N_{e,e'p}$, which is one of the strengths of this experimental method. The sources of uncertainties as well as their estimation for each kinematic is provided in Table. VIII. Since the experimental setup has evolved since then, some of these uncertainties have been reevaluated, namely the acceptance loss and inelastic contamination. Table. IX lists the estimated contributions to systematic errors on the two-photon-exchange

TABLE VIII. Estimated contributions (in percent) to the systematic error on $R = f_{corr} \times N_{e,e'n}/N_{e,e'p}$. Quantities marked with * are taken from the SBS G_M^n experiment proposal [19]. The total systematic errors on R is the quadratic sum of all other errors.

Kinematic (ϵ)	(1) 0.599	(2) 0.838
Acceptance losses	0.5 %	3.0 %
Inelastic contamination	0.9 %	0.6 %
Nucleon mis-identification*	0.6 %	
Syst. error on $R = f_{corr} \times N_{e,e'n}/N_{e,e'p}$ (Quadratic sum of the errors above)	1.3 %	3.1 %

contribution (TPE). The systematics for S_c^p and $\mu_n G_E^n/G_M^n$ have already been explicited in Sec. III, and are the leading contributions to the total uncertainty.

Inelastic contamination has been reevaluated in Sec. VI B. To evaluate the upper limit on our uncertainty, we added quadratically the inelastic contamination evaluated for the proton and the neutron for each kinematics. This would be the error that we make on R if we ignore

TABLE IX. Estimated contributions to systematic error on the Rosenbluth slope.

Syst. error on p cross section ($S_c^p = \sigma_L^p/\sigma_T^p$)	0.01
Syst. error on n form factor ($\mu_n \mathrm{G}_E^n/\mathrm{G}_M^n$)	0.05
Syst. error on Rosenbluth slope (TPE)	0.012

412 the inelastic contamination in the quasi-elastic $e-n$ and $e-p$ samples. Even in this case, we

413 expect less than 1% systematic errors. Of course, we do plan to reevaluate and subtract the

414 inelastic contamination from our actual data sample, so the quoted systematic uncertainty

415 coming from inelastic contamination should be a upper limit.

416   The acceptance loss in SBS (*i.e.* the proportion of non-detected nucleons for each detected

417 electron) have been evaluated for both kinematics. They are about 10% for the $\epsilon = 0.60$

418 kinematic (meaning that for every good electron measured, we will not measure the recoil

419 nucleon 10% of the times), but they are over 30 % for the $\epsilon = 0.84$ kinematics, which is due to

420 a larger spread of the nucleon imprint. The systematic uncertainty on the acceptance loss for

421 the ratio $R = f_{corr} \times N_{e,e'n}/N_{e,e'p}$ is maximized by the proton-neutron solid angle asymmetry

422 $A_{\Delta\Omega} = \Delta\Omega_n - \Delta\Omega_p/\Delta\Omega_n + \Delta\Omega_p$. This asymmetry is about 0.5% for the $\epsilon = 0.60$ kinematic

423 (consistent with the G_M^n proposal), but goes up to 3% for the $\epsilon = 0.84$ kinematics.

VIII. BEAM TIME REQUEST

We request 48 hours total time (32 PAC hours of beam-on target) to measure the two-photon effect (and G_E^n in one-photon approximation) at $Q^2 = 4.5$ $(GeV/c)^2$ through a measurement of the cross sections of the reaction D(e,e'N) at a large value of the virtual photon polarization ϵ=0.84. *The measurement at $Q^2 = 4.5$ $(GeV/c)^2$, ϵ=0.60 is already scheduled as part of the SBS G_M^n experiment E12-09-019* [19].

We plan to take 12 hours of data at a full luminosity of 2.86×10^{38} $cm^{-2}s^{-1}$, which corresponds to a beam intensity of $I_{exp} = 30$ μA on a liquid deuterium target with length $l_{tgt} = 15$ cm and density $d_{tgt} = 0.169$ g.cm^{-3}. To have a better handle on our backgrounds, we also plan to take 12 hours of data at half luminosity (basically by lowering the beam intensity by a factor 2). In each of these configurations, we also need to take data on a "dummy" target (*i.e.* on a target cell identical to the one used for production, but empty) to understand the contamination of our data from the target walls.

In addition to this beam time, we also require 16 hours (two shifts) to change the experimental configuration. This configuration change means:

- BigBite spectrometer angle and distance change;

- Beam pass change (from 4.4 GeV/2 pass to 6.6 GeV/3 pass);

If this experiment is approved, we plan to insert this experiment in the GMn E12-09-019 run plan in such a way that we can avoid a change in configuration for the SBS magnet and the HCal, which is very time consuming. Table. X displays an excerpt of the GMn run plan, and points out where the nTPE measurement inserts. The beam pass change and the BigBite move may be done in parallel, and should take one shift (eight hours). We require an additional shift (eight hours) for beam tuning after beam pass change. The projected use of this time is summarized in Table. XI.

This experiment will take place in Hall A, along the already scheduled SBS G_M^n experiment E12-09-019, utilizing the BigBite spectrometer to detect electrons scattered off the liquid deuterium target, and HCal calorimeter to detect the recoiling neutron and proton.

TABLE X. Excerpt of GMn E12-09-019 run plan table, showing where the $\epsilon = 0.84$ measurement would be inserted in our run plan. The $\epsilon = 0.60$ measurement is also emphasized in blue.

Step #	task	Q^2 (GeV/c)^2	θ_{BB} / θ_{SBS} degrees	Beam GeV	Time hours	Tech work time (h)
4b (install GEn-RP)	GEn-RP		41.9 / 24.7	-	4	4
4c (GEn-RP)	Production	4.5	41.9 / 24.7	4.4	104 (calendar) (52 PAC hours)	
4d (remove GEn-RP)	GEn-RP		41.9 / 24.7	-	56	24
4e (GMn/nTPE low ϵ)	Production	4.5	41.9 / 24.7	4.4	64 (calendar) (32 PAC hours)	
5a (conf. change)	BB/SBS/HCal		32.5 / 31.1	-	32	16
5b (beam tune)	beam		32.5 / 31.1	4.4	4	
5c (GMn)	Production	3.5	32.5 / 31.1	4.4	64 (calender) (32 PAC hours)	
6a (pass change)	beam/BB		23.2 / 31.1	6.6	8	4
6b (beam tune)	beam		23.2 / 31.1	6.6	8	
6c see Table. X	Production	4.5	23.2 / 31.1	6.6	64 (calendar) (32 PAC hours)	
7a (conf. change)	BB/SBS/HCal		58.4 / 17.5		32	16
+ (pass change)	beam		58.4 / 17.5	4.4	during SBS move	
7b (beam tune)	beam	-	58.4 / 17.5	4.4	4	
7c	Production	5.7	58.4 / 17.5	4.4	50 (calendar) (25 PAC hours)	

Data taking (if approved by PAC48) will take place in summer 2021 during the approved and scheduled run of the GMn, E12-09-019, experiment, which is going to measure the $e-n$ elastic scattering cross section at $Q^2 = 4.5$ (GeV/c)^2 at ϵ=0.60.

The set of instrumentation and required beam current for proposed measurement is iden-

TABLE XI. Summary table for the beam time request. Setting changes include SBS and BigBite angles change, as well as a beam pass change from 4.4 GeV (2 pass) to 6.6 GeV (3 pass). This beam pass change can mostly be done in parallel to the SBS

Task	Target	I_{exp}	time requested
Data taking (Prod.)	15 cm LD_2	30 μA	12 hours
Data taking (Syst.)	15 cm "Dummy"	30 μA	4 hours
Data taking (Prod.)	15 cm LD_2	15 μA	12 hours
Data taking (Syst.)	15 cm "Dummy"	15 μA	4 hours
Setting changes (BigBite move, beam pass change)			8 hours
Beam tune after beam pass change			8 hours
Total			**48 hours**

tical to one in the GMn experiment. The beam energy of 6.6 GeV will be used. One of two data points required for the cross section LT separation is already in the data taking plan of GMn.

There are no other measurements of TPE in the $e - n$ elastic scattering and knowledge of the TPE is essential for the understanding of the elastic electron scattering from neutron (and proton) and hadron structure. Furthermore, it is a necessary input in the analysis and interpretation of a wide range of electron scattering processes.

The kinematics of our measurements emphasize the same Q^2 range where TPE in $e - p$ elastic scattering was observed to dominate in Rosenbluth slope. Measuring at this high momentum transfers will provide unique input for testing TPE calculations [4].

We propose to measure the Rosenbluth slope and extract (in one-photon approximation) $\delta G_E^n / G_M^n$ to an accuracy of 0.15, which would bring its precision to a level comparable with that of the double polarization experiments GEN-RP and GEN-He3 at such value of Q^2. Such precision should be sufficient to detect the TPE contribution to the $e - n$ Rosenbluth slope on the three sigma level.

[1] R. Hofstadter, Rev. Mod. Phys. **28**, 214 (1956).

[2] M. N. Rosenbluth, Phys. Rev. **79**, 615 (1950).

[3] E. Christy *et al.*, "Two-photon exchange in electron-proton elastic scattering at large four-momentum transfer," (2020), in preparation for publication in PRL.

[4] P. G. Blunden, W. Melnitchouk, and J. A. Tjon, Phys. Rev. **C72**, 034612 (2005), arXiv:nucl-th/0506039 [nucl-th].

[5] J. Arrington, P. G. Blunden, and W. Melnitchouk, Prog. Part. Nucl. Phys. **66**, 782 (2011), arXiv:1105.0951 [nucl-th].

[6] A. Afanasev, P. Blunden, D. Hasell, and B. Raue, Prog. Part. Nucl. Phys. **95**, 245 (2017), arXiv:1703.03874 [nucl-ex].

[7] B. Wojtsekhowski, in *Exclusive processes at high momentum transfer. Proceedings, Newport News, USA, May 15-18, 2002* (2002) arXiv:1706.02747 [physics.ins-det].

[8] G. D. Cates, C. W. de Jager, S. Riordan, and B. Wojtsekhowski, Phys. Rev. Lett. **106**, 252003 (2011), arXiv:1103.1808 [nucl-ex].

[9] C. D. Roberts, M. S. Bhagwat, A. Holl, and S. V. Wright, Eur. Phys. J. ST **140**, 53 (2007), arXiv:0802.0217 [nucl-th].

[10] J. Segovia, I. C. Cloet, C. D. Roberts, and S. M. Schmidt, Few Body Syst. **55**, 1185 (2014), arXiv:1408.2919 [nucl-th].

[11] B. Wojtsekhowski (2020) arXiv:2001.02190 [nucl-ex].

[12] G. A. Miller, Phys. Rev. Lett. **99**, 112001 (2007), arXiv:0705.2409 [nucl-th].

[13] C. E. Carlson and M. Vanderhaeghen, Phys. Rev. Lett. **100**, 032004 (2008), arXiv:0710.0835 [hep-ph].

[14] D. Muller, D. Robaschik, B. Geyer, F. M. Dittes, and J. Horejsi, Fortsch. Phys. **42**, 101 (1994), arXiv:hep-ph/9812448 [hep-ph].

[15] X.-D. Ji, Phys. Rev. Lett. **78**, 610 (1997), arXiv:hep-ph/9603249 [hep-ph].

[16] A. V. Radyushkin, Phys. Lett. **B380**, 417 (1996), arXiv:hep-ph/9604317 [hep-ph].

[17] M. Diehl and P. Kroll, Eur. Phys. J. **C73**, 2397 (2013), arXiv:1302.4604 [hep-ph].

[18] N. Kivel, (2020), private communications.

[19] J. Annand, R. Gilman, B. Quinn, B. Wojtsekhowski, *et al.*, unpublished. See `https://www.jlab.org/exp_prog/proposals/09/PR12-09-019.pdf`, `https://www.jlab.org/exp_prog/proposals/proposal_updates/PR12-09-019_pac35.pdf` (2008).

[20] E. B. Hughes, T. A. Griffy, M. R. Yearian, and R. Hofstadter, Phys. Rev. **139**, B458 (1965).

[21] R. G. Arnold *et al.*, Phys. Rev. Lett. **61**, 806 (1988).

[22] L. Durand, Phys. Rev. **115**, 1020 (1959).

[23] E. E. W. Bruins *et al.*, Phys. Rev. Lett. **75**, 21 (1995).

[24] G. Kubon *et al.*, Phys. Lett. **B524**, 26 (2002), arXiv:nucl-ex/0107016 [nucl-ex].

[25] J. Lachniet *et al.* (CLAS), Phys. Rev. Lett. **102**, 192001 (2009), arXiv:0811.1716 [nucl-ex].

[26] V. Punjabi, C. F. Perdrisat, M. K. Jones, E. J. Brash, and C. E. Carlson, Eur. Phys. J. **A51**, 79 (2015), arXiv:1503.01452 [nucl-ex].

[27] A. Puckett, unpublished. See `https://hallaweb.jlab.org/wiki/index.php/Documentation_of_g4sbs` (2016).

[28] D. E. Wiser, "Photoproduction of protons, kaons and pions at slac energies," Ph.D. thesis, University of Wisconsin (1977).